Exploiting Electrocorticographic Spectral Characteristics for Optimized Signal Chain Design: A 1.08 μW Analog Front End with Reduced ADC Resolution Requirements

William A. Smith, *Student Member, IEEE* Brian J. Mogen, Eberhard E. Fetz, Visvesh S. Sathe, *Member, IEEE*, Brian P. Otis, *Senior Member, IEEE*

***Abstract*—Electrocorticography (ECoG) is an important area of research for Brain-Computer Interface (BCI) development. ECoG, along with some other biopotentials, has spectral characteristics that can be exploited for more optimal front-end performance than is achievable with conventional techniques. This paper optimizes noise performance of such a system and discusses an equalization technique that reduces the analog-to-digital converter (ADC) dynamic range requirements and eliminates the need for a Variable Gain Amplifier (VGA). We demonstrate a fabricated prototype in 1p9m 65nm CMOS that utilizes the results of this analysis, and verify that it records with fidelity. This prototype takes advantage of the presented findings to achieve high-fidelity, full-spectrum ECoG recording. It requires 1.08 μW for a 150 Hz bandwidth for the entire analog front end and only 7 bits of ADC resolution.**

***Index Terms*—electrocorticography, neural amplifier, ECoG, flicker noise, biopotential, low-power**

I. Introduction

Electrocorticography (ECoG), the recording of aggregate neuronal activity at the surface of the cortex, is a powerful technique for acquiring cortical information. ECoG has historically been used in the treatment of epilepsy to pinpoint the locus of seizures, but has recently become an interesting area of study for Brain-Computer Interface (BCI) research [1].

While neural activity is often measured by directly observing individual neurons, there is significant information contained in the local field potential (LFP), which is the sum of a large number of neural activities aggregated into slowly moving extracellular potential changes. The LFPs can be recorded in different ways. The most invasive is penetrating electrodes, which pierce the pial surface of the cortex and provide the highest spatial resolution. The least invasive, electroencephalography (EEG) relies on measurements from outside the skull on the surface of the skin, and does not require surgery, but has significantly lower spatial resolution and signal amplitude. ECoG represents an advantageous middle ground between these two extremes. ECoG requires surgery but does not involve the extensive brain trauma and subsequent tissue response produced by penetrating electrodes; the technique can still capture important neural information with the high spatial and temporal resolution critical for BCI research. [2].

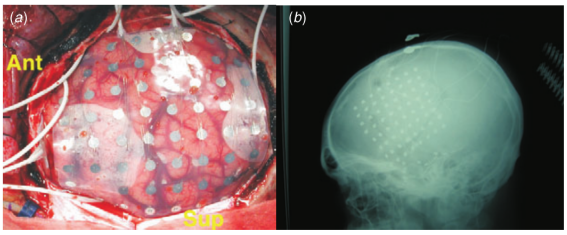

Figure 1. A ECoG electrode grid implanted in human subject [9]. (a) shows a photograph of the implanted array. (b) is an x-ray of the patient's skull. © IOP Publishing. Reproduced by permission of IOP Publishing. All rights reserved

ECoG instrumentation both in the lab and in the clinic has some critical drawbacks for BCI research. The recording equipment is rack mounted with long tethers connected to the subjects. This measurement setup is problematic because it makes it difficult for the subject to behave naturally, induces motion artifacts, and limits recording times; additionally, long-term transdermal connections commonly cause chronic infection. As a result of these requirements, there is a need for high-density wireless ECoG recording sensor systems. There has been significant research effort into this problem in recent years [3]–[8].

Most existing systems are designed to be agnostic to unique ECoG signal characteristics, primarily, the inversely proportional relationship between signal power and frequency. In this paper, we discuss two ways to exploit the spectral characteristics of ECoG. The first is a new target for ECoG amplifier noise based on the unique spectral characteristics and use cases for ECoG data. The second is to differentiate the input ECoG signal before digitization in order to reduce the dynamic range requirements of the ADC. We demonstrate a prototype utilizing these approaches with prerecorded and in-vivo results.

In Section II we discuss nature, utility, and future needs of ECoG for BCI applications. Section III discusses properties

This work was supported by the W. M. Keck Foundation and NIH grant RO1-NS12542.

W. Smith, V. Sathe, and B. Otis are with the University of Washington Department of Electrical Engineering. B. Otis is also with GoogleX. (e-mail: wasmith2@uw.edu)

B. Mogen is with the University of Washington Department of Bioengineering (e-mail: mogenb@uw.edu)

E. Fetz is with the University of Washington Department of Physiology and Biophysics

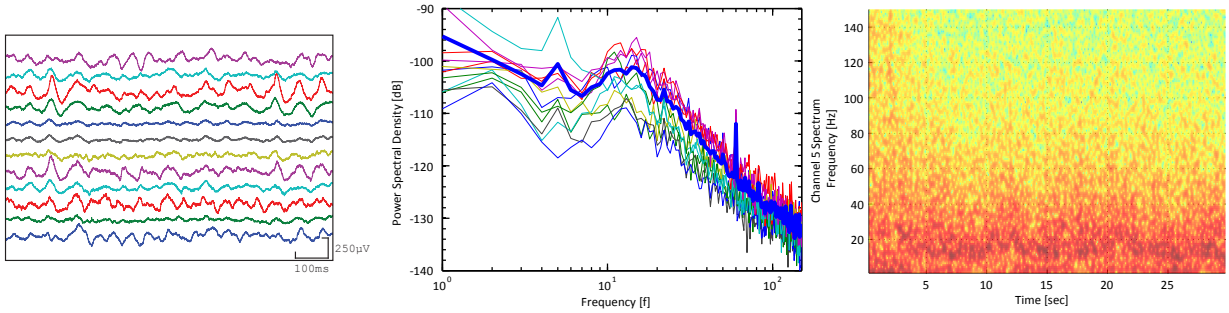

(a) (b) (c)

Figure 2. Characteristics of recorded ECoG from an awake macaque monkey. (a) One second of ECoG data. (b) PSD of 30 seconds of ECoG data. The bold line corresponds to the PSD mean of 12 channels. (c) Spectrogram corresponding to one channel of (b). Data was recorded on a g.USB Biosignal Amplifier (Guger Technologies, Graz Austria), AC coupled with a 10 mHz cutoff frequency sampled at 4.8 kHz

of ECoG that can be exploited for optimal front-end design. Section IV describes the prototype developed to test these ideas, and Section V describes the prototype test results. Section VI shows the prototype recording in-vivo, and finally Section VII draws conclusions from this work.

II. Electrocorticography Overview

ECoG has been a powerful tool for studying the function of the brain since the 1950s. It was developed by neurosurgeons Wilder Penfield and Herbert Jasper, who used electrical recordings from the surface of the brain to help locate sources of epileptic seizures and deliver electrical stimulation to map cortical function. This allowed surgeons to minimize the area of resection for epilepsy treatment [10]. In current practice, ECoG arrays are applied as a strip or grid of metal electrode pads (see Figure 1). ECoG arrays are used extensively in rodents and non-human primates; in humans it has demonstrated utility in neurophysiology and BCI research [11].

A. The Nature of ECoG Signals

Electrical activity recorded from the surface of the brain reflects a complex summation of activity from the neural tissue below the electrode. The spatial and temporal organization of neurons underneath a contact both contribute to the acquired signal. Modeling work [12] and non-human primate research [13], [14] conclude that much of the ECoG signal comes from the underlying, axially oriented pyramidal cell dipoles. From 100-10,000 cells up to 0.5 mm away contribute to the signal acquired by an electrode [15], [16]. Additional modeling shows that the primary contribution to a distant LFP comes not only from the intrinsic synaptic potentials of a population of cells but also the phase synchrony of these potentials.

A number of oscillatory components within specific frequency ranges (bands) have been described in electrocorticography. These bands reflect anatomical and functional characteristics of cortical and subcortical networks and their interactions, and they are correlated with a variety of cognitive processes and behaviors. Starting with the lowest frequency, researchers have distinguished the following bands: δ (1-4 Hz), ϑ (4-8 Hz), α (8-13 Hz), β (15-30 Hz), γ (30-60 Hz), and high-γ (>60 Hz). These rhythms have been tied to cortical activity during language production and understanding [17], [18], vision [19], movement [20], and movement planning [21], among others.

Figure 2 shows the time and frequency domain behavior of ECoG recorded from a quietly sitting macaque monkey. Its amplitude clearly shows a characteristic attenuation as a function of frequency. There is typically an increase in power spectral density (PSD) in the beta band (the 'β-bump'), and a rapid attenuation at higher frequencies, including γ and high-γ. The β band is thought to arise from the near-synchronous oscillatory firing of widespread populations of neurons, and higher frequency bands are more directly related to spatially-localized multiunit cortical activity [20], [22].

B. Utility of ECoG in BCI and Neuroscience

High-fidelity ECoG recordings have been used for a wide range of clinical applications and investigations of basic research principles. ECoG has been validated as both as a tool for investigating new phenomena in the brain as well as a viable control platform for a variety of output technologies. ECoG signals have been recorded, decoded, and/or volitionally modulated to control cursors on computer screens [1], move robotic arms for paralyzed patients [23], and decode individual finger movements [24]. For the treatment of epilepsy, ECoG activity can be used to detect pre-ictal activity and deliver electrical stimulation to preempt and stop intractable seizures [25]. In most of these applications, high-frequency components of ECoG (γ and high-γ), have consistently provided the most relevant features. These small and highly-localized signals are the most difficult to record using current technology.

C. Future Needs for Brain Computer Interfaces

Long-term recording of ECoG has been validated with a variety of clinical uses; however, one of the primary concerns with current technology is the longevity of wired systems. Electrode design and encapsulation techniques have been developed that minimize the risk of infection around implanted wires. New electrode materials and geometries have been shown to take advantage of the body's natural healing and

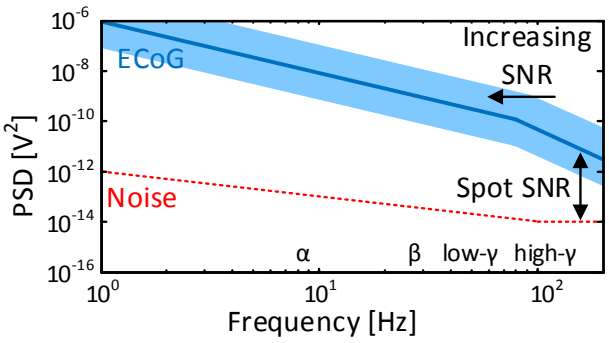

Figure 3. Typical PSD of ECoG and representative noise PSD of a low-noise amplifier [27]

defense responses to ensure that implanted systems are stable long term without signal degradation [26]. The development of power-efficient electronics for scalable, high-density, and wireless ECoG recording remains an open technical challenge.

III. Exploiting the ECoG PSD for Efficient Design

The unique frequency characteristics of ECoG and the reliance on the PSD for analysis allow for more efficient design than is possible with a conventional AFE. As seen in Figure 2 and described in Figure 3, the ECoG power spectrum does not have consistent amplitude throughout the range of frequencies. Instead, it attenuates with frequency. It has been proposed that the power spectrum decays approximately with $1/f^2$ below 80 Hz and at $1/f^4$ above [28].

We can improve circuit performance without loss in signal fidelity by taking advantage of the ECoG PSD. First, it is reasonable to neglect 1/f noise under certain conditions that will be discussed in the next section. Second, the use of an integrated noise specification typically results in overdesign. We propose an alternate spot noise target. This will reduce the amplifier power requirements by easing the amplifier noise requirements. Finally, we will show that utilizing an analog-to-digital converter (ADC) in the conventional sense is inefficient, as the quantization noise has a mostly constant PSD across frequency. A very high-resolution ADC is required to digitize the full signal range, but this can be reduced by addressing the differences between the ECoG PSD and the PSD of the ADC quantization noise. These optimizations made possible by examining the ECoG PSD can offer significant power savings and circuit complexity reduction over conventional methods.

A. Determining Requirements for SNR

The ECoG data in Figure 2 shows a strong frequency dependence, as discussed in Section II. These spectral characteristics drive analysis of ECoG signals into the frequency domain, or into sub-banded time domain slices for each of the identified ECoG bands. Consequently, a more suitable approach for determining ECoG noise requirements is to use a bandwidth appropriate to the analysis, instead of the noise integrated over the entire ECoG spectrum. In the case of spectrograms, as in Figure 2c, this is typically on the order of a 1 Hz bandwidth. For time domain analysis, the uppermost band (high-γ) has the smallest amplitude, and will drive noise requirements in the time-domain context.

Consider the the model described in [28] and shown in Figure 3. As more signal is integrated below the maximum frequency of interest, the SNR will always increase because the ratio of signal to noise increases as frequency decreases. As a result, the worst case noise requirements are at the maximum in-band frequency. Integrating the noise through the high-γ band will still be a less stringent requirement than achieving adequate SNR to properly record the highest frequency bin of the spectrogram. As a result, the spot noise at this frequency should drive the noise performance beyond that required for time-domain analysis.

Figure 4 compares the traditional integrated noise metric (from 1-150 Hz) with the spot noise metric (at 150 Hz). This analysis can be generalized to other maximum frequency choices. The contour plots show the dependence of input-referred total integrated noise and spot noise, respectively, on the input-referred thermal noise and noise corner. It is clear in Figure 4a that for integrated noise, flicker noise has a significant impact. However, in Figure 4b, flicker noise remains insignificant to approximately a 100 Hz noise corner. An integrated noise specification forces the design to account for flicker noise that may not affect performance for this application.

Secondly, compare the required input referred thermal noise for a 1 µV integrated noise target with a 100 nV/$\sqrt{\text{Hz}}$ spot noise target. A 1 uV integrated noise target requires approximately 85 nV/$\sqrt{\text{Hz}}$ of thermal noise PSD, assuming ideal elimination of flicker noise. The 100 nV$\sqrt{\text{Hz}}$ spot noise target requires 100 nV$\sqrt{\text{Hz}}$ thermal noise floor. This difference isn't that significant, but because the impact on noise-limited amplifiers of a 15% reduction in noise is quadratic, this already results in a 27% reduction in power. More importantly, ECoG research is beginning to look at higher bandwidths (e.g. 500 Hz-1 kHz) [8], and at 500 Hz the required thermal noise floor is 45 nV/$\sqrt{\text{Hz}}$. Because ECoG amplifiers are noise limited, a spot noise specification of 100 nV$\sqrt{\text{Hz}}$ could result in a four-fold decrease in power consumption. Whether the use of spot noise results in significant power savings or not, the spot noise metric is more closely coupled to the actual noise requirements for this use case than a broadband integrated noise specification, and will result in a better understanding of the system requirements.

To validate that targeting a spot noise of 100 nV$\sqrt{\text{Hz}}$ is sufficient to accurately record real data and view it in the time domain, consider Figure 5. In this figure the SNR of the average PSD shown in Figure 2b versus the designed amplifier noise specifications is shown. Note that the scale of the amplitudes in Figure 2b are considerably smaller than those seen in other work (e.g. [28]), so this represents a fairly conservative analysis. It also suggests that the spot noise target should be conservatively designed to accomodate a variety of recording scenarios, which is why we have chosen 100 nV$\sqrt{\text{Hz}}$.

Figure 5a shows that the SNR is quite high for a 100 nV$\sqrt{\text{Hz}}$

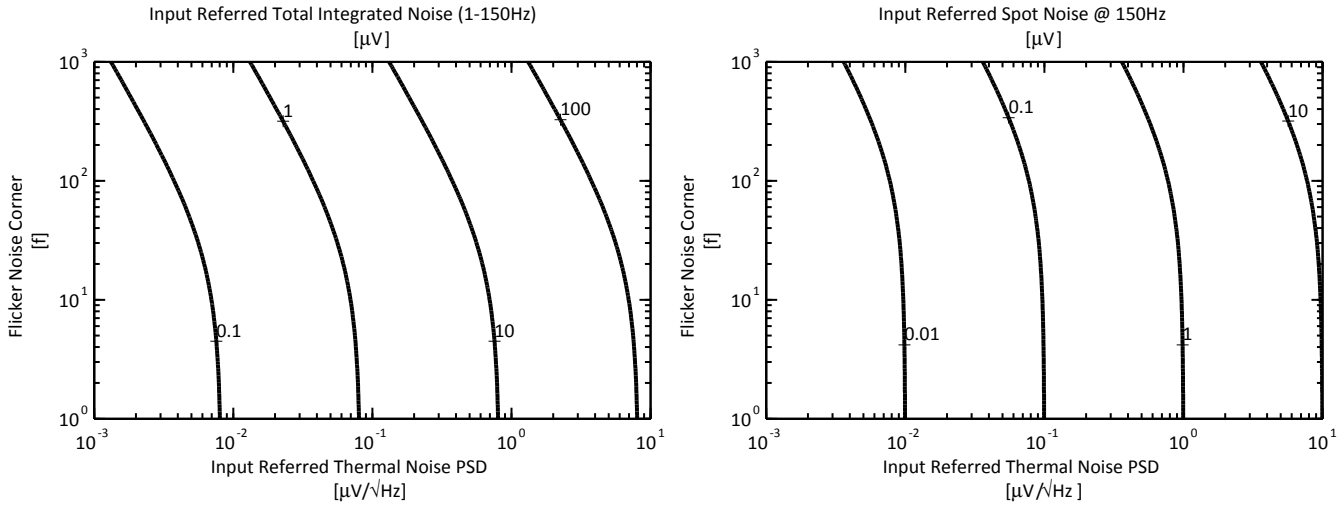

(a) Integrated noise plotted against both thermal and flicker noise

(b) Spot noise plotted against both thermal and flicker noise

Figure 4. Comparing the difference in required noise performance when utilizing a total integrated noise target from 1-150 Hz versus targeting the spot noise at 150 Hz.

thermal noise floor with a 100 Hz noise corner. There is considerable dependence on the flicker noise, but the SNR is still sufficient ($>$ 30 dB). Figure 5b shows that even these relatively small signals still have more than 10 dB of SNR under the designed conditions. As a point of reference, the mean PSD of Figure 2b at 150 Hz is 260 nV/$\sqrt{\text{Hz}}$ RMS, giving a spot SNR of 8.3 dB at 150 Hz.

Given this new spot noise target, the traditional noise efficiency factor (NEF) expression [29] must be altered slightly. The resulting expression is shown in Equation 1.

$$\text{Spot NEF} = V_{n,spot}\sqrt{\frac{2I_{tot}}{\pi \cdot V_T \cdot 4kT}} \tag{1}$$

The results of this analysis are twofold. First, there is no need to try to suppress 1/f noise if the maximum-frequency SNR is sufficient. Second, overall noise requirements for the amplifier can be relaxed to reduce amplifier power consumption. In this paper we show a prototype that validates both of these assumptions.

B. Optimizing ADC Resolution Requirements

With ECoG PSD characterized by the $1/f^2$ and $1/f^4$, the SNR at the maximum frequency is much smaller than the total SNR required across frequencies. This leads to inflated ADC requirements to accommodate the entire signal range simultaneously. A highly calibrated variable-gain amplifier (VGA)

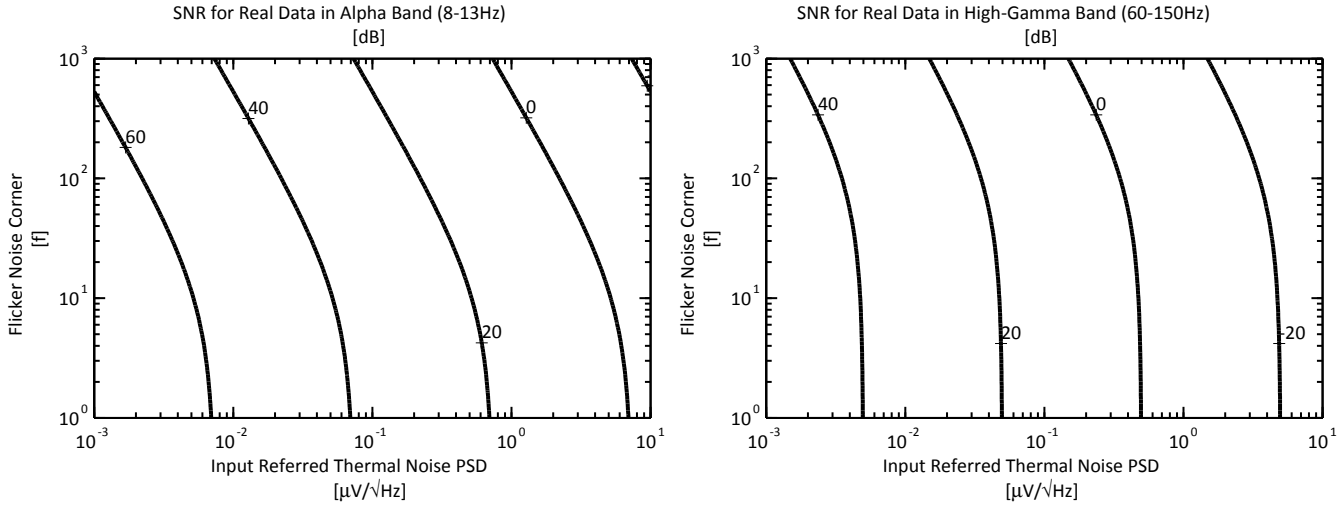

(a) SNR in the α band of real data from Figure 2b plotted against both thermal and flicker noise

(b) SNR in the high-γ band of real data from Figure 2b plotted against both thermal and flicker noise

Figure 5. SNR for a designed level of noise performance in the α and high-γ bands. The plot clearly shows that the SNR is quite high in the α band for any choice that achieves good SNR in the high-γ band. It also shows that the high-γ band is relatively insensitive to the noise corner as long as that noise corner is not significantly higher than the band itself.

can somewhat mitigate these requirements by ensuring that the entire ADC range is used for a given channel (eliminating the variable amplitude from electrode to electrode). A VGA combined with a tunable high-pass filter can be used, but in this case the entire ECoG spectrum is not simultaneously available; this significantly decreases the utility for BCI.

The full dynamic range of the ADC can be utilized at all frequencies by reshaping the waveform into a signal with a more consistent amplitude across the frequency spectrum. One simple way to equalize the signal spectrum is to perform differentiation. This, to first-order, makes the resulting spectrum white because the signal is primarily proportional to $1/f^2$. After differentiation and digitization, the signal can be recovered with low overhead using a digital integrator. The primary component of signal amplitude variation, the variation across frequency, is dramatically reduced by equalizing this spectrum before digitization. Differentiation of a signal decreases the amplitude of the signal by an additional 20 dB for each decade of frequency range. Over the range from 1-150 Hz, this reduces the low frequency content by 43dB with respect to the high-frequency signal. Because the high-frequency signal is more than 43dB below the low-frequency signal, this ideally results in a 43 dB reduction in dynamic range, which corresponds to more than 6 bits of ADC resolution.

The idea of preemphasizing parts of the ECoG spectrum is not new. In [30] the authors create a pre-emphasis at high-γ signal frequencies. This technique has a particular corner frequency that must be precisely calibrated for proper reconstruction. In another case, [5], the authors sub-band the data at different frequencies before digitization, which also reduces the total signal dynamic range but precludes native viewing the entire ECoG band. In [31], the authors describe a "folding" technique, where the signal is reset to a default DC value when it increases beyond a threshold. This technique requires significant post-processing to recover the original signal, but can reduce the ADC resolution requirement.

In [32] the authors show the efficacy of implementing a high-pass corner at 100 Hz using discrete devices, and proves that highly reliable reconstruction is possible. This technique is also utilized in [33] for a penetrating electrode recording system using a switch capacitor filter to implement the high-pass corner. By performing this operation in the first stage, the authors reduce the size of the required input capacitors by relaxing the high-pass corner requirements of the system. This can significantly reduce the chip area of an amplifier channel, as these amplifiers are typically limited by the size of the AC coupling capacitors at their input. However, when the spectrum shaping is implemented in the first stage, the amplifier's flicker noise becomes the dominant contributor to SNR degradation at low frequencies.

C. Proposed Signal Chain

One way of implementing this analog-differentiator, digital-integrator scheme is shown in Figure 6. It utilizes the Low-Noise Amplifier (LNA) then VGA neural amplifier scheme first proposed in [34] and widely used since, but replaces the VGA with an analog high-pass filter with a corner above the maximum frequency desired, which serves as a differentiator. By placing the spectrum shaping circuit in the second stage, we reduce the noise requirements of the first stage and can apply the ideas presented in Section III-A. After the ADC, data is recovered by a digital accumulator, recovering a very accurate version of the original signal with relaxed ADC requirements and without the need for VGA calibration.

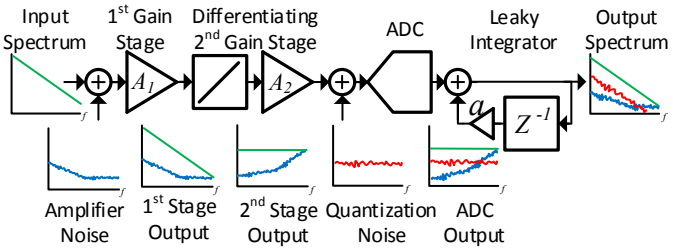

Figure 6. Conceptual block diagram of signal chain [27]

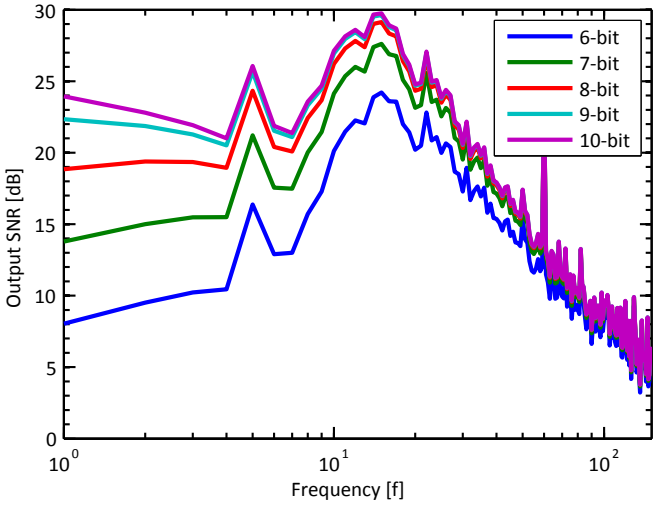

Figure 7. Plot of output referred SNR versus both physical and quantization noise for the average PSD shown in Figure 2b. The quantization noise was calculated using V_{ref} = 1 V and f_s = 500 Hz. At N = 6, the signal begins to degrade significantly.

To understand how quantization affects the overall SNR of the system when it is shaped as described in Figure 6, consider Figure 7. This figure shows the output-referred SNR of the average PSD in Figure 2b versus frequency for electrical and quantization noise over several different quantization levels. ECoG signals satisfy all of Bennett's Criteria [35], and therefore the quantization noise can be considered to be random, which results in the familiar quantization noise PSD $V^2 = V_{LSB}^2/12f_s$. This is analyzed along with thermal noise to produce Figure 7, which shows that for $N < 7$, the system begins to significantly degrade the signal. The most significant degradation occurs at low frequency. The precise quantization level needed will depend on the spectral content of the channel. This data has a much smaller amplitude than the model in [28] and weakens at low frequency, as can be seen in Figure 2b with relatively low power in the δ and ϑ bands. Thus, the SNR is lower at very low frequencies while our model would have

predicted a constant SNR. As previously stated, this suggests that there is considerable variability in ECoG signals, and design should be conservative.

Using this technique, we have eliminated the need for a VGA and have reduced the required ADC resolution. Eliminating the VGA still yields significant ADC resolution savings because the VGA addresses variability in signal amplitude between channels and across time, while the differentiator addresses the variability in signal amplitude from low-to-high frequencies.

Elimination of the VGA is critical for large-scale ECoG systems, because individually tuning hundreds of amplifier channels is an intractable problem. While this system does not directly address the channel to channel variation of the signal that makes a VGA necessary, it does reduce the dynamic range of an individual channel. This makes the need for precisely controlled dynamic range less important, which allows for a greater tolerance in second stage gain. This allows designers to remove the VGA without having to significantly overdesign dynamic range. Our implementation, as shown conceptually in Figure 6 does not have a VGA.

Automatic gain control (AGC) is an alternative method for eliminating individual VGA tuning [36], [37], but it requires complicated digital control schemes that consume additional power. Converting a gain stage into a differentiating stage does not nominally consume any additional power. In reality, implementing both an AGC scheme and this differentiation scheme would minimize the required ADC resolution. These schemes are complimentary if the resulting reduction in ADC power from the AGC scheme is larger than the power consumed by the AGC scheme itself.

IV. Prototype Amplifier Design

Figure 8 shows the constructed front-end block diagram. The first amplifier stage is an LNA that uses capacitive feedback to AC couple the signal with pseudoresistors to create a high-pass corner below 1 Hz. C_1 and C_2 were sized to produce 40 dB of gain in the pass band. The amplifier was compensated to produce a low-pass pole at 250 Hz to ease the antialiasing filter requirements, making the overall stage have a bandpass response.

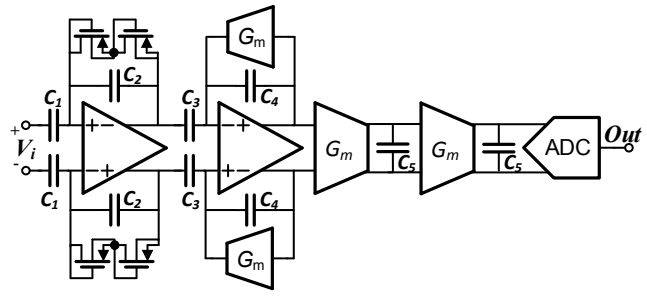

Figure 8. Block diagram of prototype ECoG signal chain with off-chip ADC. Modified from [27]. C_1 = 20 pF, C_2 = 200 fF, C_3 = 10 pF, C_4 = 100 fF, C_5 = 400 fF

The second stage performs the differentation of the input signal. The stage is similar to the first, but instead of pseudoresistors it utilizes G_m cells to create a high-pass corner at 200 Hz. This filter serves as a differentiator for all signals in the passband. Once again, the stage is compensated to place a pole at 250 Hz to ease antialiasing requirements.

After amplification and conditioning the signal is additionally antialiased in two successive G_mC filters and is then ready to be digitized with an ADC.

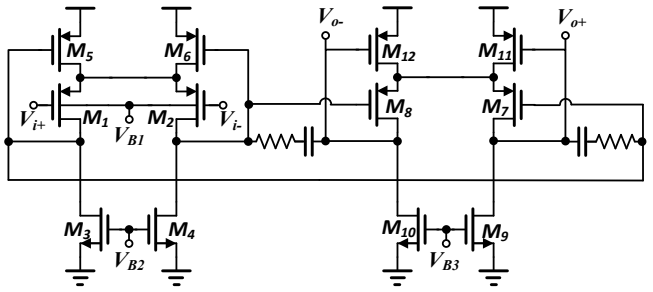

Figure 9. Opamp topology for both amplifier stages [27]

The transistor-level schematic of the first- and second-stage operational amplifiers is shown in Figure 9. The topology is identical for both stages, but they differ in bias conditions and transistor geometry because of their different performance requirements. The topology utilizes tail current source based common-mode feedback for both stages, making both the first and second stage of the op-amp self-biased and fully differential. While less linear than resistive sensing of the common-mode, this scheme is practically realizable for ultra-low-power amplifiers and does not require an external common mode feedback voltage. Additionally, using this self-biased scheme, there is no additional current consumed for the comparison of common mode voltage. The amplifier operates from a supply voltage of 1 V, but all devices are 2.5 V I/O devices to reduce gate leakage for these large and low-bias-current devices.

In the first stage, the bias current and device geometry are increased in the M_1, M_2 legs for improved 1/f and thermal noise performance. This stage has a forward biased bulk voltage V_{B1} to reduce the required V_{ov} of these devices. The amplifiers are compensated for stability using standard lead compensation.

V. Prototype Measurement Results

The prototype discussed in Section IV was fabricated in a 1p9m 65 nm CMOS process. A die photo of the resulting IC is shown in Figure 10. While the chip was fabricated with an ADC on-chip, we bypassed this ADC for the purposes of this paper in order to better understand ADC requirements. A single ECoG amplifier channel is on the chip with dimensions of 511 µm by 167 µm.

The resulting transfer function and noise performance for the fabricated chip are shown in Figure 11. The amplifier has a 40 dB/decade high-pass filter for low frequencies that decreases to 20 dB/decade high-pass at 0.5 Hz. This 20 dB/decade high-pass corresponds to integration in the signal band of interest. Above the maximum frequency of 150 Hz several poles from the amplifier compensation and antialias filtering orchestrate an 80 dB/decade rolloff. The input referred

Table I
PERFORMANCE COMPARISON OF PROTOTYPE WITH OTHER ECOG AFES

	JSSC'07 [3]	JSSC'08 [4]	TCAS'11 [5]	ESSCIRC'13 [7]	ISSCC'14 [8]	This Work
Power per channel (μW)	2	6.9	3.2	36.3[3]	2.3[3]	1.08
Spot Noise[1] ($nV/\sqrt{Hz}$)	100	55	80	—	58	112
Spot NEF[1]	3.88	3.21	5.56	—	4.83	4.52
Spot PEF[1,2]	27.10	30.91	37.10	—	11.66	20.43
CMRR (dB)	100	120	80	87	—	82
PSRR (dB)	—	—	60	90	—	68
AFE Bandwidth (Hz)	0.005-180	0.5-100	0.4-200	—	1-500	0.5-150
ADC Resolution	—	11-bit[4]	8-bit[5]	16-bit[6]	15-bit	7-bit[7]
Area (mm^2/ch)	0.8	0.45	0.4[8]	—	0.025	0.085
VGA	Yes	Yes	Yes	No	No	No
Supply Voltage (V)	1.8	3	1.2	3.3	0.5	1
Technology	0.8 μm	0.5 μm	130 nm	0.6 μm	65 nm	65 nm

[1] At 150 Hz, except [4], which is at 100 Hz
[2] $NEF^2 \cdot VDD$ [38]
[3] Includes bias circuits
[4] EEG amplifier
[5] Sub-bands signal to reduce resolution
[6] Direct digital conversion from multiplexed array
[7] Based on analysis in Section V
[8] Requires off-chip filter

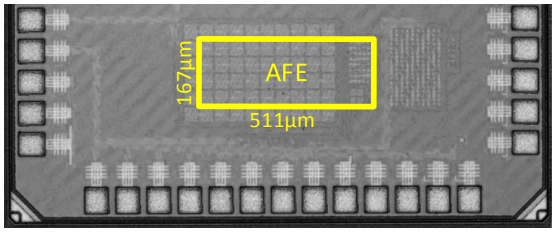

Figure 10. Fabricated die photo [27]

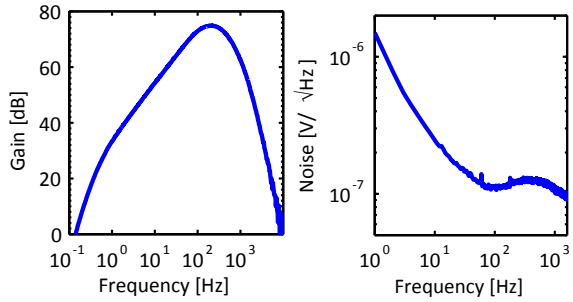

Figure 11. Measured AFE magnitude response and input-referred noise PSD [27]

noise plot in Figure 11b shows that 1/f noise is present, as expected, and that the system achieves a noise floor of 112 $nV/\sqrt{Hz}$ at 150 Hz, the designed maximum frequency of interest. This measurement is close to the designed target of 100 $nV/\sqrt{Hz}$ discussed in Section II.

A. Signal Fidelity Testing

A first comparison of prerecorded ECoG data with the same data run through this prototype system is shown in Figure 12a. This figure shows good fidelity ($r > 0.9$) throughout the frequency range except at the lower end of the spectrum. The discrepancy is due to saturation in the first amplifier stage for large, low-frequency signal content. This is especially prevalent during large motion artifact events, which is not a primary concern as this is work toward a future fully-implanted system, which will not be subject to the same large scale motion artifacts. These motion artifacts are a part of the prerecorded data, and are due to the test setup used to record the data on an awake and moving macaque monkey.

This plot primarily shows that the particular prototype does not have enough dynamic range to accommodate a signal as large as the prerecorded data used without some saturation. In simulation, the 1% THD of the front-end is 4 mV peak-to-peak, which is typically sufficient for ECoG applications. However, this particular dataset has spikes as large as 8 mV peak-to-peak.

By reducing the PSD of the same channel's signal by a factor of 2 before it is input to the amplifier, as seen in Figure 12b (with a slight time shift), we see that the correlation issues at low frequencies disappear, and we end up with a very high overall correlation rate of r = 0.9729. There is no strong frequency component to the correlation. This result supports the hypothesis that saturation is the root cause of the poorly correlated low-frequency signal, and suggests that the gain of the LNA stage should be lower in order to accomodate signals larger than 4 mV peak-to-peak. This would increase the power required for the first stage.

B. Required ADC Resolution

Figure 13 shows how the correlation between the prerecorded spectra in Figures 12a and 12b is affected by the number of bits used for digitization. This experiment was

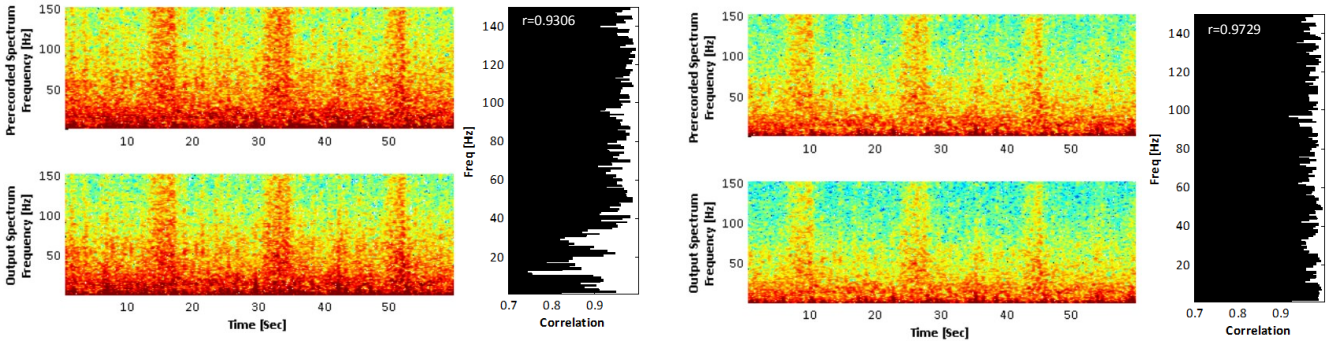

(a) (b)

Figure 12. Comparison of prerecorded data to same data after processing with AFE. (a) represents data in original form, while (b) represents data from the same channel with doubled signal power that verifies the low-frequency saturation hypothesis.

conducted via post-processing in Matlab using various quantization levels assuming a 1 V referenced ADC. In all cases the data were sampled at 1 ksps. For the original waveform, correlation is highly consistent down to 6-bits, and below 6 bits there is deterioration of the signal quality.

In the scaled waveform shown in Figure 12b, correlation is degraded somewhat earlier, below 7-bits of resolution. This is expected for a direct scaling of the original signal. 7-bit ADC resolution is still sufficient to achieve high fidelity (r = 0.97) to the prerecorded data.

C. Comparison to State-of-the-Art

Table I shows the results of this prototype compared to other ECoG recording designs. This system achieves the lowest power per channel of the listed amplifiers. This is not primarily due to more efficient amplifier design, as the spot-NEF and spot-PEF figures show. Instead, we have reduced the power requirements by targeting an appropriate noise specification as discussed in Section III.

Most of the other specifications are comparable to other state-of-the-art works, but note that this system is capable of being digitized by a 7-bit ADC. This is significantly lower than any other system with the exception of [5], which sub-bands the data and does not allow for simultaneous recording of full-spectrum ECoG. Note that most other systems without a VGA require substantially higher ADC resolution. Our system outperforms all listed systems at full signal reconstruction.

VI. In-Vivo Measurement Results

In addition to the prerecorded data used in Section V, the prototype AFE was also tested in-vivo on a non-human primate to verify that the system is capable of recording electrophysiological data in a normal preparation. A sedated macaque monkey with previously implanted 250um platinum/iridium rod electrodes placed over primary motor cortex was connected to the prototype amplifier using approximately 12 inches of unshielded wire. The positive amplifier terminal was connected to a surface electrode and the negative terminal was connected to the ground screw located in the animal's skull. Sixty seconds of data was recorded through the amplifiers and output to

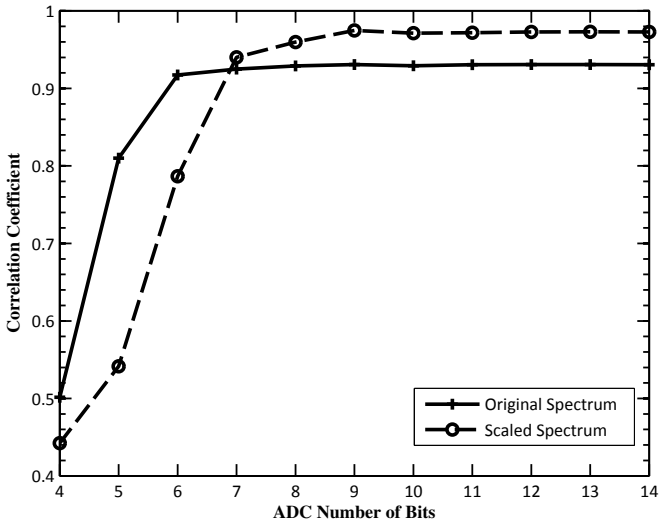

Figure 13. Change in correlation with ADC resolution for the prerecorded ECoG data in Figure 12a and Figure 12b.

an external ADC. The resulting spectrograms and PSD, both before and after integration, are shown in the Figures 14 and 15, respectively.

As can be seen from the figure, the amplifier successfully records in-vivo neural data. The signal shows a characteristic decay with frequency (once recovered with integration). There is a significant 60 Hz peak on the amplifier output caused by the unshielded inputs, but they do not saturate the amplifier. Additionally, there is a second harmonic at 120 Hz, approximately 30dB below the first harmonic. This is caused by differences between the active and reference electrode wire lengths, which differentially couple 60 Hz and its harmonics to the amplifier input. Both the 60 Hz and 120 Hz harmonics are due to conditions imposed by the test environment available for this experiment. As shown in Figure 12, the system has sufficient CMRR and PSRR to reject 60 Hz in situations where the input leads are well matched.

Before integration, the signal has approximately 18 dB of dynamic range. After integration, the recovered signal has

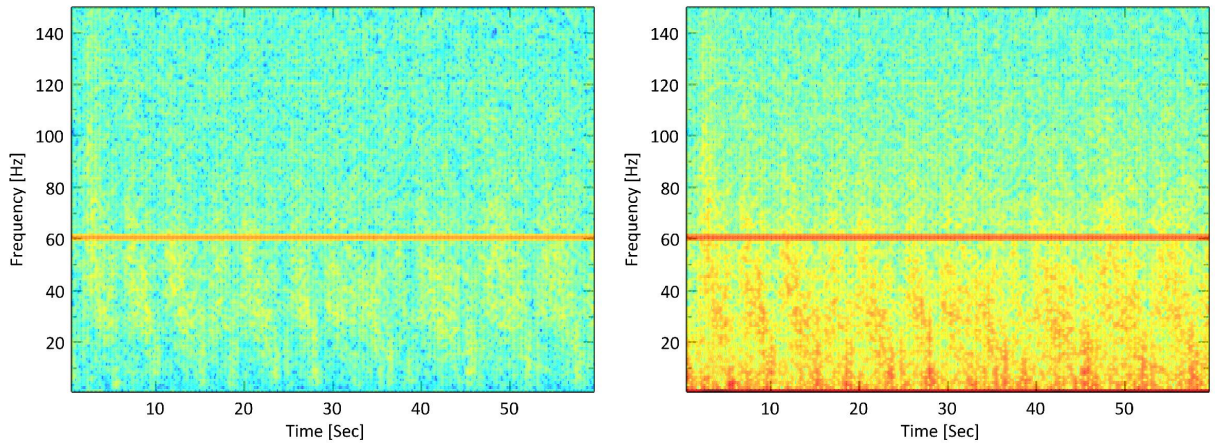

(a) Spectrogram of amplifier output before integration

(b) Spectrogram of amplifier output after integration

Figure 14. Spectrogram at amplifier output of 60 s of in-vivo recording of a sedated macaque monkey using the prototype chip before and after integration.

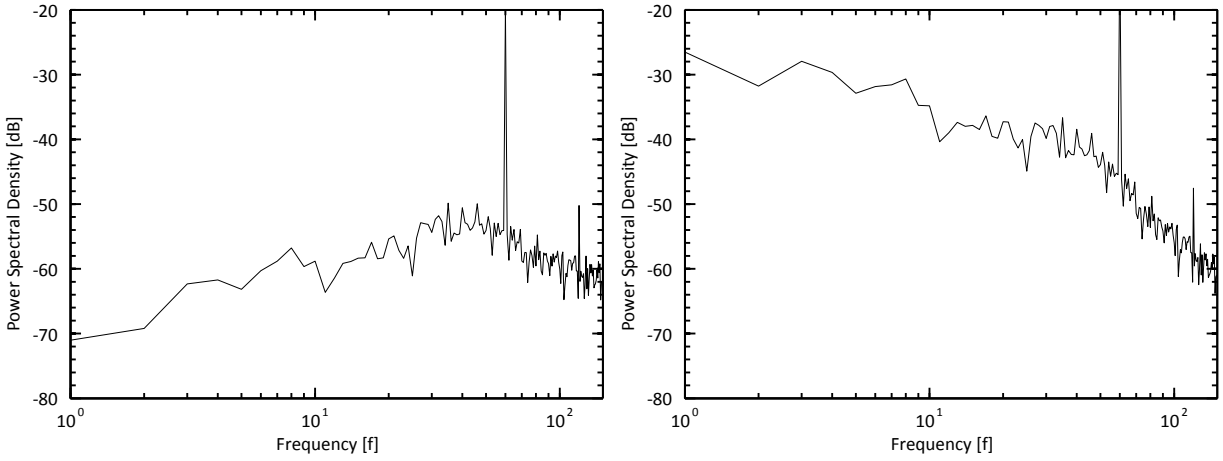

(a) Before integration

(b) After integration

Figure 15. PSD of output spectrograms presented in Figure 14. This figure shows a characteristic neural signature in (b)

35 dB of dynamic range, so in this particular case the ADC dynamic range required is approximately half of that required for a normal AFE.

VII. Conclusion

In this paper we have discussed techniques for AFE design specific to electrocorticography. Amplifier efficiency can be improved by properly accounting for performance as it relates specifically to the signal of interest. We have shown that it is possible to decrease the required ADC resolution to 7-bits while simultaneously eliminating the need for a VGA. We have also shown that the noise performance requirements of ECoG are much less aggressive than are typically implemented on neural interface chips, which led to power savings in this prototype, and can potentially yield significant additional savings if these findings are utilized more aggressively and over larger frequency ranges. Our differentiation technique has been successfully implemented for ECoG, and could have utility for other biopotentials that have similar underlying PSD characteristics. Reducing the power budget for recording channels is highly desirable, especially for high-density wireless recording, so these improvements will assist in enabling future wireless high-density ECoG recording systems.

Acknowledgements

The authors would like to thank Dr. Stavros Zanos for helpful discussions on the nature and application of ECoG potentials.

References

[1] G. Schalk, K. J. Miller, N. R. Anderson, J. a. Wilson, M. D. Smyth, J. G. Ojemann, D. W. Moran, J. R. Wolpaw, and E. C. Leuthardt, "Two-dimensional movement control using electrocorticographic signals in humans." *Journal of Neural Engineering*, vol. 5, no. 1, pp. 75–84, Mar. 2008.

[2] K. J. Miller, S. Zanos, E. E. Fetz, M. den Nijs, and J. G. Ojemann, "Decoupling the cortical power spectrum reveals real-time representation of individual finger movements in humans," *The Journal of Neuroscience*, vol. 29, no. 10, pp. 3132–3137, 2009.

[3] T. Denison, K. Consoer, W. Santa, A.-T. Avestruz, J. Cooley, and A. Kelly, "A 2 μW 100 nV/rtHz Chopper-Stabilized Instrumentation Amplifier for Chronic Measurement of Neural Field Potentials," *IEEE J. Solid-State Circuits*, vol. 42, no. 12, pp. 2934–2945, Dec 2007.

[4] R. Yazicioglu, P. Merken, R. Puers, and C. Van Hoof, "A 200 μW Eight-Channel EEG Acquisition ASIC for Ambulatory EEG Systems," *IEEE J. Solid-State Circuits*, vol. 43, no. 12, pp. 3025–3038, Dec 2008.

[5] F. Zhang, A. Mishra, A. Richardson, and B. Otis, "A Low-Power ECoG/EEG Processing IC with Integrated Multiband Energy Extractor," *IEEE Trans. Circuits Syst. I, Reg. Papers*, vol. 58, no. 9, pp. 2069–2082, Sept 2011.

[6] S. Robinet, P. Audebert, G. Regis, B. Zongo, J.-F. Beche, C. Condemine, S. Filipe, and G. Charvet, "A Low-Power 0.7 mv_{rms} 32-Channel Mixed-Signal Circuit for ECoG Recordings," *IEEE J. Emerging Sel. Topics Circuits Syst.*, vol. 1, no. 4, pp. 451–460, Dec 2011.

[7] S. Ha, J. Park, Y. Chi, J. Viventi, J. Rogers, and G. Cauwenberghs, "85 db dynamic range 1.2 mW 156 kS/s biopotential recording IC for high-density ECoG flexible active electrode array," in *Proc. ESSCIRC 2013*, Sept 2013, pp. 141–144.

[8] R. Muller, H.-P. Le, W. Li, P. Ledochowitsch, S. Gambini, T. Bjorninen, A. Koralek, J. Carmena, M. Maharbiz, E. Alon, and J. Rabaey, "A miniaturized 64-channel 225 μW wireless electrocorticographic neural sensor," in *Tech. Dig. IEEE ISSCC 2014*, Feb 2014, pp. 412–413.

[9] E. C. Leuthardt, G. Schalk, J. R. Wolpaw, J. G. Ojemann, and D. W. Moran, "A brain-computer interface using electrocorticographic signals in humans." *Journal of Neural Engineering*, vol. 1, no. 2, pp. 63–71, Jun. 2004.

[10] W. Penfield and H. Jasper, *Epilepsy and the functional anatomy of the human brain.* Oxford, England: Little, Brown & Co., 1954.

[11] G. Schalk and E. C. Leuthardt, "Brain-computer interfaces using electrocorticographic signals." *IEEE Reviews in Biomedical Engineering*, vol. 4, pp. 140–54, Jan. 2011.

[12] H. Lindén, T. Tetzlaff, T. C. Potjans, K. H. Pettersen, S. Grün, M. Diesmann, and G. T. Einevoll, "Modeling the spatial reach of the LFP." *Neuron*, vol. 72, no. 5, pp. 859–72, Dec. 2011.

[13] N. Murthy, E. E. Fetz, V. N. Murthy, and E. E. Fetz, "Synchronization of neurons during local field potential oscillations in sensorimotor cortex of awake monkeys." *Journal of Neurophysiology*, vol. 76, no. 6, pp. 3968–82, Dec. 1996.

[14] A. K. Engel, P. König, A. K. Kreiter, T. B. Schillen, and W. Singer, "Temporal coding in the visual cortex: new vistas on integration in the nervous system," *Trends in Neurosciences*, vol. 15, no. 6, pp. 218–226, Jun. 1992.

[15] P. L. Nunez and R. Srinivasan, *Electric Fields of the Brain: The Neurophysics of EEG*. Oxford University Press, 2006.

[16] G. Buzsáki, C. a. Anastassiou, and C. Koch, "The origin of extracellular fields and currents–EEG, ECoG, LFP and spikes." *Nature reviews. Neuroscience*, vol. 13, no. 6, pp. 407–20, Jun. 2012.

[17] N. E. Crone, L. Hao, J. Hart, D. Boatman, R. Lesser, R. Irizarry, and B. Gordon, "Electrocorticographic gamma activity during word production in spoken and sign language," *Neurology*, vol. 57, no. 11, pp. 2045–2053, Dec. 2001.

[18] N. E. Crone, D. Boatman, B. Gordon, and L. Hao, "Induced electrocorticographic gamma activity during auditory perception," *Clinical Neurophysiology*, vol. 112, no. 4, pp. 565–582, Apr. 2001.

[19] B. M. Harvey, M. J. Vansteensel, C. H. Ferrier, N. Petridou, W. Zuiderbaan, E. J. Aarnoutse, M. G. Bleichner, H. C. Dijkerman, M. J. E. van Zandvoort, F. S. S. Leijten, N. F. Ramsey, and S. O. Dumoulin, "Frequency specific spatial interactions in human electrocorticography: V1 alpha oscillations reflect surround suppression." *NeuroImage*, vol. 65, pp. 424–32, Jan. 2013.

[20] K. J. Miller, E. C. Leuthardt, G. Schalk, R. P. N. Rao, N. R. Anderson, D. W. Moran, J. W. Miller, and J. G. Ojemann, "Spectral changes in cortical surface potentials during motor movement." *The Journal of Neuroscience*, vol. 27, no. 9, pp. 2424–32, Feb. 2007.

[21] N. E. Crone, D. L. Miglioretti, B. Gordon, and R. P. Lesser, "Functional mapping of human sensorimotor cortex with electrocorticographic spectral analysis. II. Event-related synchronization in the gamma band," *Brain*, vol. 121, no. 12, pp. 2301–2315, Dec. 1998.

[22] N. E. Crone, A. Sinai, and A. Korzeniewska, "High-frequency gamma oscillations and human brain mapping with electrocorticography," in *Event-Related Dynamics of Brain Oscillations*, ser. Progress in Brain Research, C. Neuper and W. Klimesch, Eds. Elsevier, 2006, vol. 159, pp. 275 – 295.

[23] T. Yanagisawa, M. Hirata, Y. Saitoh, H. Kishima, K. Matsushita, T. Goto, R. Fukuma, H. Yokoi, Y. Kamitani, and T. Yoshimine, "Electrocorticographic control of a prosthetic arm in paralyzed patients." *Annals of Neurology*, vol. 71, no. 3, pp. 353–61, Mar. 2012.

[24] J. Kubánek, K. J. Miller, J. G. Ojemann, J. R. Wolpaw, and G. Schalk, "Decoding flexion of individual fingers using electrocorticographic signals in humans." *Journal of Neural Engineering*, vol. 6, no. 6, p. 066001, Dec. 2009.

[25] F. T. Sun, M. J. Morrell, and R. E. Wharen Jr., "Responsive Cortical Stimulation for the Treatment of Epilepsy," *Neurotherapeutics*, vol. 5, no. 1, pp. 68–74, Jan. 2008.

[26] A. A. Schendel, M. W. Nonte, C. Vokoun, T. J. Richner, S. K. Brodnick, F. Atry, S. Frye, P. Bostrom, R. Pashaie, S. Thongpang, K. W. Eliceiri, and J. C. Williams, "The effect of micro-ECoG substrate footprint on the meningeal tissue response." *Journal of Neural Engineering*, vol. 11, no. 4, p. 046011, Aug. 2014.

[27] W. Smith, B. Mogen, E. Fetz, and B. Otis, "A spectrum-equalizing analog front end for low-power electrocorticography recording," in *European Solid State Circuits Conference (ESSCIRC), ESSCIRC 2014 - 40th*, Sept 2014, pp. 107–110.

[28] K. Miller, L. Sorenson, J. Ojemann, and M. den Nijs, "Power-Law Scaling in the Brain Surface Electric Potential," *PLoS Comput. Biol.*, vol. 5, no. 12, December 2009.

[29] M. Steyaert and W. Sansen, "A micropower low-noise monolithic instrumentation amplifier for medical purposes," *IEEE J. Solid-State Circuits*, vol. 22, no. 6, pp. 1163–1168, Dec 1987.

[30] A. Mishra, F. Zhang, and B. Otis, "ElectroCorticoGraphy (ECoG) acquisition exploiting signal characteristics for reduced power," in *IEEE BioCAS 2011*, Nov 2011, pp. 37–40.

[31] Y. Chen, A. Basu, L. Liu, X. Zou, R. Rajkumar, G. Dawe, and M. Je, "A digitally assisted, signal folding neural recording amplifier," *IEEE Trans. Bio. Circuits Sys.*, vol. 8, no. 4, pp. 528–542, Aug 2014.

[32] S. Venkatraman, C. Patten, and J. Carmena, "Exploiting the 1/f structure of neural signals for the design of integrated neural amplifiers," in *IEEE EMBC 2009*, Sept 2009, pp. 2050–2053.

[33] J. Xu, T. Wu, W. Liu, and Z. Yang, "A frequency shaping neural recorder with 3 pf input capacitance and 11 plus 4.5 bits dynamic range," *IEEE Trans. Biomed. Circuits Syst.*, vol. 8, no. 4, pp. 510–527, Aug 2014.

[34] R. Harrison and C. Charles, "A low-power low-noise cmos amplifier for neural recording applications," *IEEE J. Solid-State Circuits*, vol. 38, no. 6, pp. 958–965, June 2003.

[35] R. Jacob Baker, *CMOS Mixed-Signal Circuit Design*. Wiley, 2009.

[36] R. Rieger and S.-L. Deng, "Double-differential recording and agc using microcontrolled variable gain asic," *Neural Systems and Rehabilitation Engineering, IEEE Transactions on*, vol. 21, no. 1, pp. 47–54, Jan 2013.

[37] S. Paraskevopoulou and T. Constandinou, "An ultra-low-power front-end neural interface with automatic gain for uncalibrated monitoring," in *Circuits and Systems (ISCAS), 2012 IEEE International Symposium on*, May 2012, pp. 193–196.

[38] R. Muller, S. Gambini, and J. Rabaey, "A 0.013 mm^2 , 5 μW , dc-coupled neural signal acquisition ic with 0.5 v supply," *Solid-State Circuits, IEEE Journal of*, vol. 47, no. 1, pp. 232–243, Jan 2012.